Contents lists available at ScienceDirect

The International Journal of Biochemistry & Cell Biology

Different microRNA alterations contribute to diverse outcomes following EV71 and CA16 infections: Insights from high-throughput sequencing in rhesus monkey peripheral blood mononuclear cells

Yajie Hu [1], Jie Song [1], Longding Liu, Jing Li, Beibei Tang, Jingjing Wang, Xiaolong Zhang, Ying Zhang, Lichun Wang, Yun Liao, Zhanlong He, Qihan Li (MD, PhD)*

Institute of Medical Biology, Chinese Academy of Medical Science and Peking Union Medical College, Kunming 650118, China

ARTICLE INFO

ABSTRACT

Enterovirus 71 (EV71) and Coxsackievirus A16 (CA16) are the predominant pathogens of hand, foot, and mouth disease (HFMD). Although these viruses exhibit genetic homology, the clinical manifestations caused by the two viruses have some discrepancies. In addition, the underlying mechanisms leading to these differences remain unclear. microRNAs (miRNAs) participate in numerous biological or pathological processes, including host responses to viral infections. Here, we focused on differences in miRNA expression patterns in rhesus monkey peripheral blood mononuclear cells (PBMCs) infected with EV71 and CA16 at various time points using high-throughput sequencing. The results demonstrated that 106 known and 13 novel miRNAs exhibited significant differences, and 32 key miRNAs among them for target prediction presented opposite trends in the EV71- and CA16-infected samples. GO and pathway analysis of the predicted targets showed enrichment in 14 biological processes, 10 molecular functions, 8 cellular components and 104 pathways. Subsequently, regulatory networks of miRNA-transcription factors, miRNA-predicted targets, miRNA-GOs and miRNA-pathways were constructed to reveal the complex regulatory mechanisms of miRNAs during the infection phase. Ultimately, we analysed hierarchical GO categories of the predicted targets involved in immune system processes, which indicated that the innate and adaptive immunity following EV71 and CA16 infections may be remarkably distinct. In conclusion, this report is the first describing miRNA expression profiles in PBMCs with EV71 and CA16 infections using high-throughput sequencing. Our findings could provide a valuable basis for further studies on the regulatory roles of miRNAs related to the different immune responses caused by EV71 and CA16 infections.

© 2016 The Authors. Published by Elsevier Ltd. This is an open access article under the CC BY-NC-ND license (http://creativecommons.org/licenses/by-nc-nd/4.0/).

1. Introduction

Enterovirus 71 (EV71) and Coxsackievirus A16 (CA16) both belong to the human enterovirus A (HEV-A) species of the Picornaviridae family and are the predominant aetiological agents of hand, foot, and mouth disease (HFMD), which frequently occurs in infants and children under 5 years of age (Mao et al., 2014; Solomon et al., 2010). HFMD is normally asymptomatic or manifests as a clinically mild and self-limited disease characterized by a brief febrile illness; typical vesicular rashes on the palms, soles, or buttocks; and

oropharyngeal ulcers (Aswathyraj et al., 2016). However, in the last few decades, HFMD has caused several outbreaks in the Asia-Pacific region with high numbers of deaths and severe central nervous system complications, including aseptic meningitis, cerebella ataxia, poliomyelitis-like paralysis, acute brainstem encephalitis, and fulminant neurogenic pulmonary edema (Aswathyraj et al., 2016; Koh et al., 2016; Muehlenbachs et al., 2015). Thus, HFMD has resulted in increasing socio-economic burdens and has become a pressing global public health problem. Although EV71 and CA16 are both small, non-enveloped viruses containing a single-stranded RNA genome (7.4 kb) of positive polarity, and although both viruses share similar genetic homology, different clinical manifestations are caused by infections with these viruses (Mao et al., 2014; Solomon et al., 2010). Compared to CA16, EV71 infection more often results in neurological disease and sometimes even death, especially among children under 5 years old (Lee et al., 2009;

Mao et al., 2014; McMinn, 2002). Therefore, many studies have focused on EV71 and the studies of CA16 were previously largely ignored. Moreover, an inactivated EV71 vaccine developed in mainland China has successfully completed phase III clinical trials and entered into the market (Li et al., 2014a,b; Liu et al., 2014a). This vaccine was shown to be safe and to provide protection against clinical EV71-associated HFMD, but it does not have cross-strain protective activity against HFMD induced by CA16 infection (Li et al., 2014a; Liu et al., 2014a). Nevertheless, it has recently been reported that about half of the increasingly sporadic HFMD cases and outbreak events with high lethality in China have been caused by EV71 and CA16 circulating alternatively or together (Liu et al., 2014b). Additionally, CA16 infection can also initiate severe health issues and even lead to death(Mao, Wang, 2014). Hence, further investigations into the underlying molecular mechanisms of EV71 and CA16 infections in the host and additional assessments of virus-host interactions are required to develop new and better vaccines to enable broad and effective protection against, and potentially eradication of, HFMD.

microRNAs (miRNAs), endogenously encoded single-stranded RNAs of approximately 20–23 nucleotides in length, act as key regulators of gene expression at the post-transcriptional level by targeting messenger RNAs (mRNAs) for translational repression or degradation (Ha and Kim, 2014; Winter et al., 2009). Recent studies revealed that miRNAs have unique expression profiles in cells from the innate and adaptive immune systems and play pivotal roles in the regulation of both cell development and function (Carissimi et al., 2009; Xiao and Rajewsky, 2009). Furthermore, aberrant expression of miRNAs results in dysregulated innate and adaptive immunity, which can cause autoimmune diseases and haematopoietic malignancies (Carissimi et al., 2009; Lee et al., 2014). Therefore, miRNAs have been widely used as diagnostic and prognostic indicators of disease type and severity in recent years. Additionally, it has become increasingly clear that host-encoded miRNAs can positively or negatively regulate virus life cycles by directly interacting with target sites in viral transcripts or by modulating cellular gene expression, which alters host physiology, including components of the immune system (Louten et al., 2015). Moreover, accumulating research has indicated that virally encoded miRNAs can regulate viral or cellular gene expression and therefore contribute to viral replication and pathogenesis (Powdrill et al., 2016; Sharma and Singh, 2016). Thus, delineating the emerging roles of cellular and virus-encoded miRNAs in host-pathogen interactions may lead to the development of new antiviral therapies that work by manipulating such regulatory molecules.

Numerous studies have indicated that EV71 infection can influence host miRNA expression profiles and that changes in these profiles are involved in antiviral responses and immune escape in EV71 infection (Ho et al., 2016). In addition, our previous study verified that EV71 and CA16 infections trigger remarkable alterations in the immune response, which could be the reason why diverse clinical features are caused by the individual pathogens(Song et al., 2016; Zhang et al., 2014). Hence, based on the above studies, we hypothesized that the host miRNAs that are induced by CA16 infection might be distinct from those that are induced by EV71 infection. Furthermore, although EV71 and CA16 infections stimulate many common miRNAs, some miRNAs that are induced show opposite expression trends between infections with the two viruses. Peripheral blood mononuclear cells (PBMCs), consisting of lymphocytes (T cells, B cells and NK cells), monocytes and dendritic cells, are thought to be an essential component of the immune system, and alterations in PBMC populations are most likely linked to the clinical features that occur during the progression of viral infection (Delves et al., 2006). Therefore, we utilized high-throughput sequencing of miRNA expression profiles in rhesus monkey PBMCs infected with EV71 and CA16 to investigate why these viruses result in diverse immune responses and clinical features. The results from this study could provide new perspectives regarding the mechanisms underlying EV71 and CA16 pathogenesis.

2. Materials and methods

2.1. Cell culture and virus infection

PBMCs were isolated from EDTA-anticoagulated whole blood samples from healthy rhesus monkeys with no known infections or diseases. The PBMCs were isolated by Ficoll-Hypaque gradient centrifugation according to the manufacturer's instructions. Then, PBMCs plated onto 6-well plates at 2×10^5 cells per well were cultivated in RPMI 1640 medium (Gibco, USA) supplemented with 10% foetal bovine serum (FBS, Gibco, USA) plus penicillin and streptomycin and incubated overnight at 37 °C in 5% CO_2 in a humidified incubator. The EV71 virus strain (sub-genotype C4, GenBank: EU812515.1) that originated from an epidemic in Fuyang, China in 2008 and the CA16 virus G20 strain (sub-genotype B, GenBank: JN590244.1), which originated from an HFMD patient in Guangxi in 2010, were propagated in PBMCs at a multiplicity of infection (MOI) of 1 the following day. Cells were infected in triplicate and collected at 0, 24 and 48 h post infection (hpi). Cells infected with EV71 and CA16 for 0 hpi were used as controls. We defined the different experimental groups as EV71–0 h, EV71–24 h, EV71–48 h, CA16–0 h, CA16–24 h and CA16–48 h. Additionally, a subset of the EV71–0 h and CA16–0 h groups were subjected to normalization (the normalization value was set to 1), and these two groups were then designated Con.

2.2. miRNA extraction from PBMCs and quality control

miRNA extraction from each group of cells was performed using standard mirVana™ miRNA Isolation Kit (Ambion, USA) protocols. RNA integrity was then evaluated using RNA 6000 Nano LabChips on an Agilent 2100 Bioanalyzer (Agilent Technologies, USA). To further confirm RNA quality, the total RNA degradation was estimated by reviewing electropherograms and the RNA integrity number (RIN) of each sample. Only samples with preserved 18S and 28S peaks and RIN values greater than 7 were selected for miRNA profile analysis. Qualified miRNA samples from three independent experiments of each group were pooled respectively and used for subsequent library construction and deep sequencing.

2.3. Small RNA (sRNA) library construction, sequencing and analysis

High-throughput sequencing technology, as a powerful tool for transcriptome analysis, not only detects known transcripts, but also facilitates the discovery of novel transcripts (Malone and Oliver, 2011). Small RNA library construction and sequencing was carried out by the National Engineering Center for Biochip in Shanghai on an Illumina HiSeq 2000 system. For all samples, small RNA libraries were constructed using a TruSeq Small RNA sample preparation kit (Illumina, USA) following the manufacturer's instructions and were sequenced with an Illumina Genome Analyzer II system. Adaptor sequences were first trimmed from small RNA reads. Then, low-quality sequences, namely, those with undetermined nucleotides (Ns), quality scores (Q-scores) less than 10, and reads shorter than 18nt, were discarded from all libraries. Clipped high-quality sequences were clustered into unique reads, and sRNAs with a length of 18–35nt were identified. Moreover, non-coding RNAs, including ribosomal RNA (rRNA), transfer RNA (tRNA), and small nuclear RNA (snRNA), were eliminated based on reference sequences from Rfam (http://rfam.janelia.org/) and piRNA (http://pirnabank.ibab.ac.in/). Afterward, the clean reads

were mapped to known miRNA precursors, and the mature miR-NAs were deposited in miRBase 19.0 (available online: http://www.mirbase.org/). Unmappable sequences were used to predict potentially novel candidate miRNAs with the Mfold RNA folding prediction web server (available online: http://mfold.rna.albany.edu/). The sequencing data were submitted to the Gene Expression Omnibus (GEO) database (www.ncbi.nlm.nih.gov/geo/) under the accession number GSE85820.

2.4. Bioinformatic analysis of sequencing data

2.4.1. Principal component analysis (PCA)

After data preprocessing, to explore relationships between samples, PCA plots of the samples were created using the clean data through a median centering of the data set.

2.4.2. Differential analysis of known and novel miRNAs

The samples were normalized by calculating the tags per million of total RNA reads (TPM) and used to compare the relative abundances of specific miRNAs within each data set. miRNAs with a P value ≤ 0.05 (chi-squared test) and a fold change ≥ 2 or ≤ 0.5 were considered significantly different among the groups.

2.4.3. Unsupervised hierarchical clustering

We first defined differentially expressed miRNAs using log2-fold changes in the ratios of the detected signals [log2 (infected/control)]. Then, unsupervised hierarchical clustering analyses of differentially expressed miRNAs were performed using the R computer program. Correlation similarity matrixes and complete linkage algorithms were used for the cluster analyses.

2.4.4. Trend analysis

To isolate pivotal differences between the EV71- and CA16-infected samples, we identified a set of unique expression patterns in accordance with different signal density changes in miRNAs under different situations.

2.4.5. miRNA target prediction

The potential targets of the differentially expressed miRNAs were predicted with two miRNA target prediction algorithms: TargetScan and miRDB (Lewis et al., 2003; Wong and Wang, 2015). The parameters for TargetScan and miRDB were set as the top 200 genes and a target score ≥ 80, respectively.

2.4.6. Gene ontology (GO) analysis and Kyoto encyclopedia of genes and genomes (KEGG) pathway analysis

The PANTHER (Protein ANalysis THrough Evolutionary Relationships) classification system version 9.0 was used to classify genes and proteins to facilitate high-throughput analysis. The targets of differentially expressed miRNAs were subjected to GO and KEGG pathway analysis using the PANTHER Classification System.

2.4.7. Regulatory network analysis

A single miRNA can not only provoke a chain reaction but also be regulated by various transcription factors (TFs). Therefore, analysing the correlations between TFs and miRNAs, miRNAs and targets, miRNAs and GOs, and miRNAs and pathways might reveal a fundamental biological function of miRNAs. The intricate regulatory networks identified by computational approaches could clearly delineate the roles of miRNAs. To acquire an understanding of the regulatory relationships formed by miRNAs and TFs, TFs were predicted using the Ensembl web tool, and the promoter region of the miRNA was defined as a 2-kb region up-stream of the transcription start site. Meanwhile, to further reduce false positive predictions of TFs, a relative score of ≥ 0.99 was regarded to indicate a potential TF. Thereafter, based on interactions between key

differentially expressed miRNAs and their targets, target genes and GOs, and targets and pathways, regulatory networks for miRNAs, including a miRNA-targets network, a miRNA-GOs network and a miRNA-pathways network, were constituted.

2.4.8. Hierarchical GO category analysis of target genes involved in GO-biological processes of interest

We primarily focused on the immune-related GOs. GO category trees were hierarchically constructed using the PANTHER classification system.

2.4.9. Gene co-expression network construction

The GenMANIA algorithm was applied to construct the network of immune-related target genes that were predominantly involved in the above hierarchical GO categories according to the relationships among the genes, proteins and compounds in the database.

2.5. Validation of miRNAs and miRNA target genes by quantitative RT-PCR (qRT-PCR) analysis

For further validation, we randomly selected 8 differentially expressed miRNAs for qRT-PCR analysis. miRNA expression was tested by poly (A)-tailed qRT-PCR. For each sample, 2 μg of total RNA was polyadenylated and reverse transcribed using poly(A) polymerase with a Mir-X miRNA First-Strand Synthesis Kit (Clontech, USA), in accordance with the manufacturer's instructions. Subsequently, each cDNA was amplified on a 7500 Fast Real-time PCR system (Applied Biosystems, USA) with an mRQ 3′ primer and miRNA-specific 5′ primers to quantify specific miRNA sequences; the amplifications were performed using SYBR Advantage qPCR Premix (Clontech, USA). The amplification conditions were as follows: 95 °C for 10 s, 40 cycles of 95 °C for 10 s and 60 °C for 40 s, and dissociation at 95 °C for 60 s, 55 °C for 30 s and 95 °C for 30 s. All miRNA-specific 5′ primers used in the qPCR experiments are shown in Supplementary Table S1 in the online version at DOI: 10.1016/j.biocel.2016.10.011. Samples (n = 3) were run simultaneously for each miRNA in triplicate, including a no-template control, and U6 snRNA was used as an endogenous control for normalization. The relative expression levels of each miRNA were calculated from the equation $2^{-\triangle\triangle Ct}$.

To indirectly corroborate miRNA expression, target mRNA levels were measured by qRT-PCR. Total RNA was extracted using TRIzol Reagent (TIANGEN, China) according to the manufacturer's instructions. qRT-PCR was performed using a One Step SYBR® PrimeScript^{TM} RT-PCR Kit (TAKARA, Japan). The amplification cycles consisted of 1 cycle at 42 °C for 5 min and 1 cycle at 95 °C for 10 s, followed by a two-step procedure consisting of 5 s at 95 °C and 34 s at 60 °C for 40 cycles; the reactions were run on a 7500 Fast Real-time PCR system (Applied Biosystems, USA). β-actin served as a housekeeping gene for quantitative analysis. The qRT-PCR primers used for each gene in this study are listed in Supplementary Table S2 in the online version at DOI: 10.1016/j.biocel.2016.10.011. Each sample was tested in triplicate.

2.6. MiR-146b-5p-related immune targets and downstream gene verification in CD1c+ dendritic cells (DCs) infected with EV71 and CA16

The isolation of CD1c+DCs from rhesus monkey PBMCs was performed by two magnetic separation steps according to the protocol of the CD1c (BDCA-1) Dendritic Cell Isolation Kit (non-human primate, Miltenyi Biotec, Germany). The isolated cells were collected and cultured with RPMI 1640 medium (Gibco, USA) supplemented with 10% FBS (Gibco, USA) plus penicillin and streptomycin at 37 °C in 5% CO_2 in a humidified atmosphere. The EV71 virus strain and the CA16 virus G20 strain were propagated in CD1c + DCs at an MOI of

Table 1

Details of small-RNA sequencing information and subsequent data analysis. Indicated from left to right are the numbers of reads that raw sequencing data, passed quality filtering (clean reads), the numbers of reads that passed both quality filtering, adapter filtering and length filtering (adapter-trimmed reads ≥18nt), and the number of reads that could be aligned to known Macaca mulatta pre-miRNA in miRBase 19 with perfect matches, respectively.

Sample	Raw reads	Clean reads	Adapter-trimmed reads (length > = 18nt)	Reads aligned to known Macaca mulatta pre-miRNA in miRBase 19
EV71-0h	21,213,090	20,429,979	18,835,060	2,216,832
EV71-24h	20,682,035	18,876,048	17,483,343	5,478,275
EV71-48h	19,375,992	17,760,607	16,179,654	4,873,847
CA16-0h	20,578,052	19,217,115	17,882,021	4,452,125
CA16-24h	22,046,933	20,844,283	19,688,732	7,533,577
CA16-48h	21,740,610	20,040,877	18,558,364	6,048,592

Table 2

Significantly differentially expressed miRNAs during the course of EV71 and CA16 infection.

Comparison	Known differentially expressed miRNAs			Novel differentially expressed miRNAs		
	Total	Up	Down	Total	Up	Down
EV71–24 h vs. EV71-0h	70	6	64	6	4	2
EV71–48 h vs. EV71-0h	53	4	49	10	6	4
CA16–24 h vs. CA16-0h	32	11	21	5	3	2
CA16–48 h vs. CA16-0h	38	10	28	4	2	2
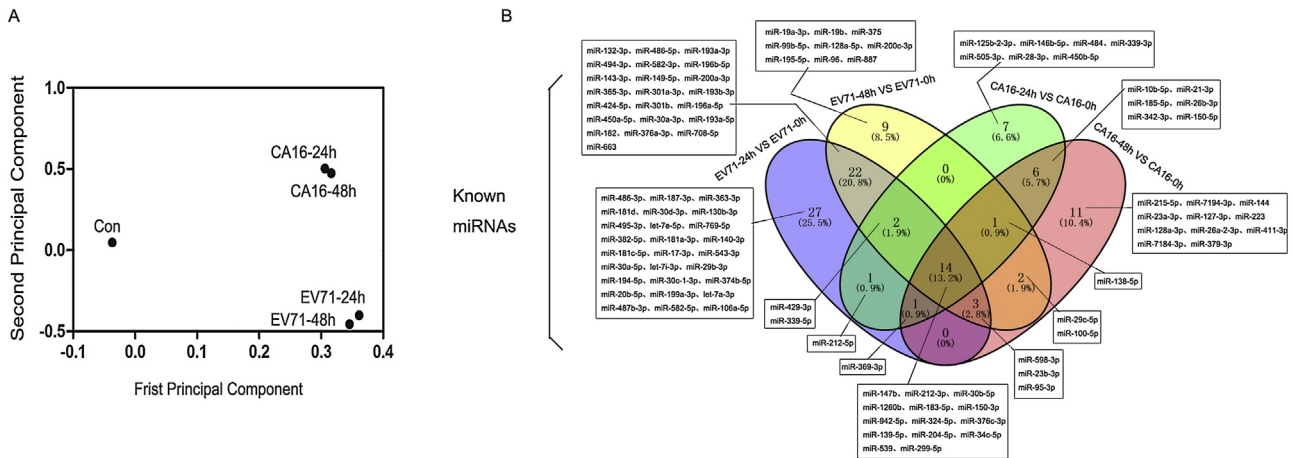
Fig. 1. Overall distribution of miRNA expression from all groups and Known differentially expressed miRNAs. (A) Overall miRNA populations are shown as a PCA plot that indicates the similarity and discrimination across all samples. EV71/CA16-infected samples were distinct from the Con sample. (B) Venn diagram showing a comparison of known differentially expressed miRNAs during infection with EV71 and CA16. Boxes show the names of differentially expressed miRNAs that were significantly changed during infection with EV71 and CA16.

1 the following day. Cells were infected in triplicate and harvested at 0, 24, 48 and 72 h post infection (hpi). Cells infected with EV71 and CA16 for 0 hpi were used as controls.

Subsequently, the extracted miRNA and mRNA of these samples were used to detect the expression levels of miR-146b-5p, its target genes (IRAK1 and TRAF6) and the molecules downstream of these targets (TNF-α, IL-1β and IL-6) by qRT-PCR. The related experimental methods are described above and the primers used to detect the miRNA and mRNAs are given in Supplementary Table S1 and S2 in the online version at DOI: 10.1016/j.biocel.2016.10. 011, respectively.

2.7. Statistical analysis

For sequencing data, raw reads obtained from each library were normalized to TPM. For qRT-PCR, the data are expressed as the mean ± standard error of mean (SEM). Statistical analysis was performed using SPSS 18.0 (IBM SPSS, USA). $P < 0.05$ was considered statistically significant.

3. Results

3.1. Global statistics of six sequenced small-RNA libraries

To determine miRNA expression patterns in response to EV71 and CA16 challenge in PBMCs, 6 small-RNA libraries from all samples were constructed and subjected to high-throughput sequencing. An overview of the miRNA-seq data processing results for all the samples is detailed in Table 1. As illustrated in Supplementary Fig. S1 in the online version at DOI: 10.1016/j.biocel.2016. 10.011, most sequences were 20–23 nucleotides in length with a peak at 22 nucleotides, which suggested that the libraries were highly enriched in miRNA sequences. Additionally, a bar chart was created to summarize the different classes of sRNAs in the samples (Supplementary Fig. S2 in the online version at DOI: 10.1016/ j.biocel.2016.10.011), and the results indicated that the miRNA expression patterns showed distinct changes at different times during EV71 and CA16 infection. To further clarify the overall variation in the samples, miRNA sequencing data were analysed by PCA (Fig. 1A). The results revealed a clear separation between the Con group and the infected groups, for both EV71 and CA16 infec-
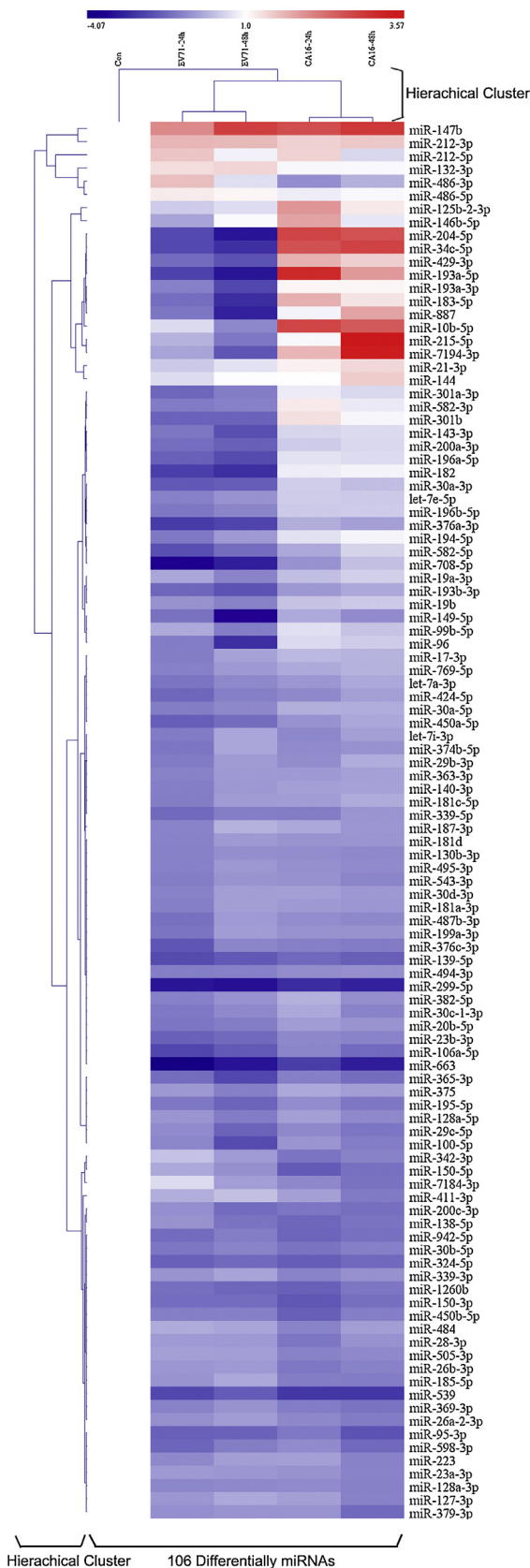
Fig. 2. Heat map diagram depicting results of the hierarchical clustering of known miRNAs and samples. The horizontal axis represents each group; the vertical axis represents expression change (log2 ratio). The color scale shows the relative expression levels of miRNA across all samples, with red showing expression levels above the mean and blue showing expression levels below the mean.

tion. Moreover, the EV71–24 h and EV71–48 h groups were clearly segregated from the CA16–24 h and CA16–48 h groups, whilst the groups infected with the same virus for different lengths of time were very similar to each other. These findings imply that a remarkable difference likely exists between the EV71-infected groups and the CA16-infected groups.

3.2. Differentially expressed miRNAs in response to EV71 or CA16 infection

Following EV71 infection, 76 differentially expressed miRNAs (including 70 known and 6 novel miRNAs) were obtained at 24 hpi based on a P value < 0.05 and a fold change ≥ 2 or ≤ 0.5. Of these, 64 known and 2 novel miRNAs were down-regulated, while 6 known and 4 novel miRNAs were up-regulated. A total of 53 known and 10 novel miRNAs were differentially expressed at 48 hpi, with 49 known and 4 novel miRNAs down-regulated and 11 known and 3 novel miRNAs up-regulated. In contrast, following infection with CA16, a relatively small number of differentially expressed miRNAs were identified in the samples. At 24 hpi, 21 known and 2 novel miRNAs were down-regulated, while 11 known and 3 novel miRNAs were up-regulated. At 48 hpi, 28 known and 2 novel miRNAs were down-regulated, and 10 known and 2 novel miRNAs were up-regulated (Table 2).

These above-described miRNAs were also represented using a Venn diagram (Fig. 1B and Supplementary Fig. S3A in the online version at DOI: 10.1016/j.biocel.2016.10.011). We observed that there were 106 known and 13 novel differentially expressed miRNAs in total across all time points during EV71 and CA16 infection. Thereafter, these 106 known and 13 novel differentially expressed miRNAs were subjected to unsupervised hierarchical clustering analysis with log fold-change values to visually illustrate the expression patterns of the miRNAs during EV71 and CA16 infection. A positive log2 value indicates up-regulation, and a negative value indicates down-regulation. The two heat maps that were generated exhibited marked discrepancies for the same strain at different times as well as for different strains at the same times following infection (Fig. 2 and Supplementary Fig. S3B in the online version at DOI: 10.1016/j.biocel.2016.10.011). This result illustrated that the known and novel miRNA expression patterns induced by EV71 and CA16 might be both strain- and time-specific.

To further confirm our sequencing data, eight significantly differently expressed miRNAs, including miR-34c-5p, miR-182, miR-582-5p, let-7i-3p, miR-150-5p, miR-147b and 2 novel miRNAs (AATTGCAGACACTAGGACT and CGAGGGGGCGGGGCGGGGTC), were chosen for qRT-PCR analysis. There were some differences in the results because of the use of different technologies, but overall we observed a general consistency between qRT-PCR and high-throughput sequencing results (Supplementary Fig. S4 in the online version at DOI: 10.1016/j.biocel.2016.10.011).

3.3. Trend analysis of differentially expressed miRNAs

To investigate the primary reasons associated with the differences between EV71 and CA16 infection, trend analysis, which explicitly took into account the temporal nature of the miRNA expression profiles, was employed to identify which predominant differentially expressed miRNAs presented an inverse expression pattern over time following EV71 and CA16 infection. As shown in Fig. 3, 35 differentially expressed known miRNAs were identified

The dendrograms show hierarchical clustering representing the similarities and dissimilarities in expression profiles among samples and miRNAs. (For interpretation of the references to colour in this figure legend, the reader is referred to the web version of this article.)

Table 3
Oppositely expressed miRNAs in response to EV71 and CA16 infection. Three miRNAs discarded are shown in red. FC, fold change.

miRNAs	EV71–24 h (FC)	CA16-24 h (FC)	Ratio (EV71-24 h/CA16-24 h)	EV71-48 h (FC)	CA16-48 h (FC)	Ratio (EV71-48 h/CA16-48 h)
miR-7194-3p	0.728386	3.073049	0.237024	0.272905	10.74647	0.025395
miR-204-5p	0.232901	6.876753	0.033868	0.109025	6.127458	0.017793
miR-183-5p	0.37592	3.210551	0.117089	0.155088	2.367415	0.065509
miR-215-5p	0.851179	1.861558	0.45724	0.423474	11.85056	0.035735
miR-147b	4.104396	6.30369	0.65111	7.082545	7.605951	0.931185
miR-34c-5p	0.228664	6.217014	0.03678	0.160278	6.918961	0.023165
miR-10b-5p	1.358487	6.752396	0.201186	0.514745	5.781785	0.089029
miR-193a-5p	0.208461	8.864564	0.023516	0.110265	3.680299	0.029961
miR-887	0.419111	1.772913	0.236397	0.129955	3.434945	0.037833
miR-144	1.362351	1.994015	0.68322	1.96256	2.68642	0.730549
miR-429-3p	0.362798	3.182151	0.11401	0.25879	2.632829	0.098293
miR-21-3p	1.097428	2.174922	0.504583	1.473674	2.525716	0.583468
miR-125b-2-3p	1.127264	3.802769	0.296432	1.397016	2.272184	0.614834
miR-193a-3p	0.473139	2.11061	0.224172	0.223922	2.103028	0.106476
miR-301b	0.321777	2.413131	0.133344	0.323322	1.840149	0.175704
miR-182	0.198514	1.670422	0.118841	0.16007	1.784112	0.08972
miR-582-3p	0.442937	2.265389	0.195524	0.473282	1.594796	0.296766
miR-146b-5p	0.730676	3.471624	0.210471	1.903475	1.557129	1.222426
miR-196b-5p	0.424724	1.105876	0.384061	0.499951	1.129597	0.442592
miR-19b	0.59551	1.032337	0.576857	0.485145	1.117267	0.434225
miR-30a-3p	0.28005	1.160452	0.241328	0.298896	0.963569	0.310197
miR-193b-3p	0.340223	0.633864	0.536744	0.263635	0.76574	0.344288
miR-582-5p	0.249021	0.768262	0.324135	0.367373	1.251302	0.293592
miR-19a-3p	0.749082	0.98331	0.761796	0.496507	1.189963	0.417246
let-7e-5p	0.475113	1.137091	0.417832	0.588858	1.107376	0.53176
miR-99b-5p	0.774337	1.414054	0.547601	0.451539	1.03465	0.436417
miR-708-5p	0.086098	0.590971	0.145688	0.125807	0.995846	0.126332
miR-376a-3p	0.189415	0.808697	0.234222	0.212905	0.69732	0.305319
miR-149-5p	0.395462	0.777593	0.508572	0.093036	0.54236	0.171539
miR-194-5p	0.43134	1.439971	0.299547	0.639778	1.793498	0.356721
miR-143-3p	0.421334	1.270905	0.331523	0.247414	1.358677	0.182099
miR-301a-3p	0.340265	1.641791	0.207252	0.456487	1.315707	0.346952
miR-200a-3p	0.374684	1.128217	0.332103	0.311651	1.304833	0.238844
miR-96	0.448406	1.329685	0.337227	0.159809	1.140893	0.140074
miR-196a-5p	0.312368	1.47114	0.212331	0.235401	1.362494	0.172772

according to the above-mentioned search method. Furthermore, it is interesting to note that these miRNAs are all separately gradually decreased and increased in EV71 and CA16 infection in the time series, suggesting that they may greatly contribute to the key distinctions induced by the two viruses. Meanwhile, it was discovered that the expression levels of the novel differentially expressed miRNAs in both EV71 and CA16 infection were either higher or lower than the Con (Fig. S3B), which indicated that there was no adverse expression tendency in the novel differentially expressed miRNAs. In total, 35 known miRNAs displayed an opposite expression tendency. To further narrow down the predominant differentially expressed miRNAs, we defined a screening criterion as follows: if the two ratios (EV71–24 h/CA16–24 h and EV71–48 h/CA16–48 h) of one of the 35 known differentially expressed miRNAs fell between 0.5 and 2, it was eliminated (Table 3). After applying this criterion, only 32 known differentially expressed miRNAs were regarded as significant.

3.4. GO and pathway analysis of predicted targets of differentially expressed miRNAs

To elucidate the possible roles of the 32 known differentially expressed miRNAs in response to EV71 or CA16 infection, the potential targets of these miRNAs were predicted with the TargetScan and miRDB programs. We found that there were 4377 genes and 2736 genes that were predicted to be potential targets with the TargetScan program and miRDB program, respectively. Only the overlapping targets identified by both programs were considered as predicted targets for each miRNA. Hence, a total of 1205 targets were identified for GO analysis. The results exhibited that these genes were categorized as follows: 14 as biological process (Fig. 4A), 10 as molecular function (Fig. 4B) and 8 as cellular

component (Fig. 4C). These results provide comprehensive information on the functions of the miRNAs in PBMCs during EV71 and CA16 infection. Next, pathway analysis based on the predicted targets revealed that the 32 miRNAs were involved in 104 pathways (Fig. 5). Among these pathways, many were intimately correlated with immune regulation (e.g., the apoptosis signalling pathway, Toll receptor signalling, T cell activation, inflammation mediated by chemokine and cytokine signalling, B cell activation, etc.) and nervous system function (e.g., axon guidance mediated by netrin, synaptic vesicle trafficking, etc.), which suggested that alterations in these miRNAs involved different immune responses and neurological symptoms induced by EV71 or CA16 infection.

3.5. miRNA regulatory networks of targets, GOs, pathways and TFs

To explore the interactions between the targets, GOs, pathways regulated by miRNAs and miRNAs mediated by TFs, we constructed regulatory networks among the miRNAs and targets, GOs, pathways, and TFs. Initially, to further narrow down the key targets, we identified intersections of related genes in GO and pathway analysis. In doing so, 151 targets were identified, as shown in Supplementary Fig. S5 in the online version at DOI: 10.1016/j.biocel.2016.10.011. Following this, 31 known differentially expressed miRNAs, 13 biological processes and 100 pathways were identified by refining the correlations between the 151 targets and the miRNAs, GOs, and pathways. Finally, the following 3 relationships were identified: 1) relationships between 31 known differentially expressed miRNAs and the 151 targets; 2) relationships between 13 GOs and the 151 targets and relationships among the 31 known differentially expressed miRNAs and 151 targets; and 3) relationships among 100 pathways and the 151 targets and relationships
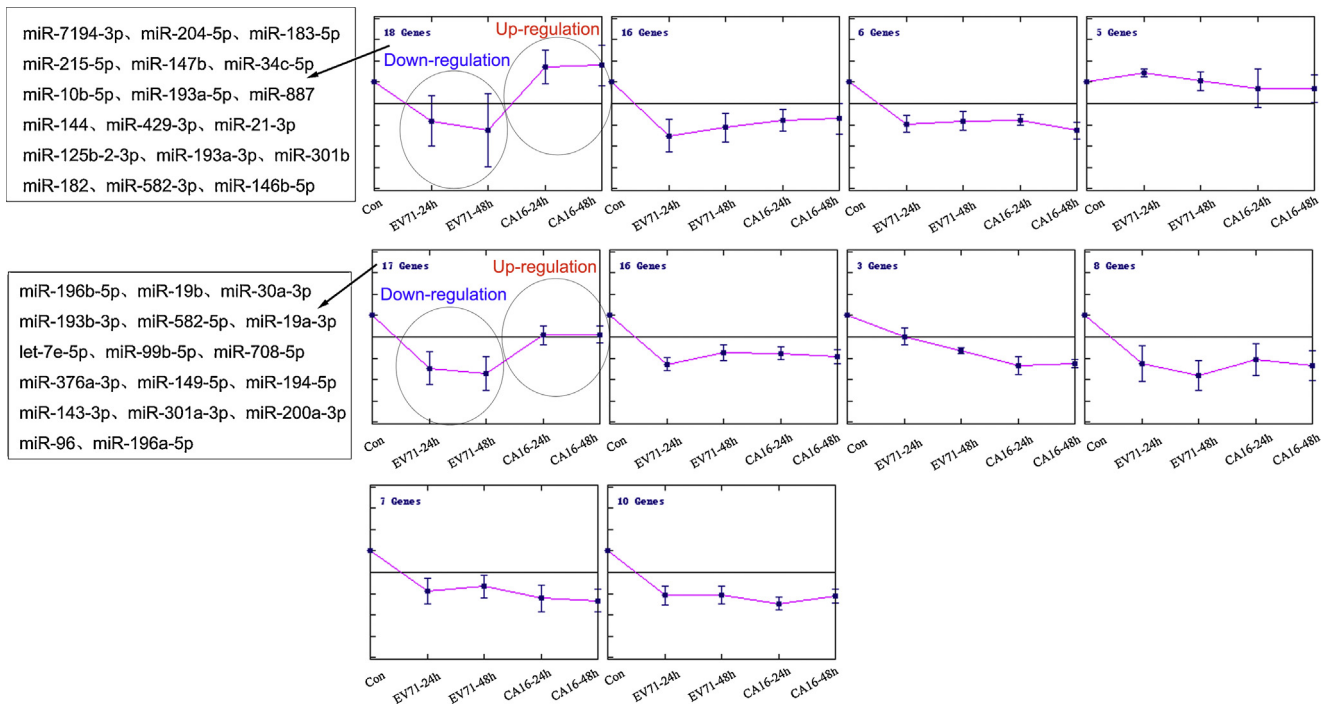
Fig. 3. Trend analysis of known differentially expressed miRNAs in response to EV71 and CA16 infection at different time points post infection. The miRNAs that showed opposite expression patterns during the progression of EV71 and CA16 infection are shown in boxes.

Table 4
Immune system processes related to miRNAs and their target genes.

miRNAs	Target genes
miR-96, let-7e-5p, miR-30a-3p, miR-582-5p, miR-204-5p, miR-19b, miR-301b, miR-19a-3p, miR-301a-3p, miR-182, miR-34c-5p, miR-200a-3p, miR-183-5p, miR-194-5p, miR-193b-3p, miR-193a-3p, miR-196a-5p, miR-196b-5p, miR-376a-3p, miR-146b-5p	TSPAN14, ADRA2C, STRBP, FAS, NRCAM, DAB2, NPTX1, FHL1, CNTFR, IGSF11, CALCR, WASL, IRF4, NUMB, ADRB2, SERP1, STAU1, PHLDB2, TSPAN12, ZFR, CCL18, IRAK1, IL15, IGDCC4, ABHD14A, ABL2, FASLG, ACER2, COLEC12, LEF1, PLAU, NOX3, CRELD1, ABCB9, PAPPA, CX3CL1, EDNRB, DCDC2, ROBO2, MAP3K13, MAPK8, RUNX3, ABHD5, TRAF6, IGDCC3, MAPK8IP1, GAB1, PPARG

among the 31 known differentially expressed miRNAs and 151 targets. Using this information, we built 3 regulatory network diagrams, including a miRNA-gene network, a miRNA-GO network and a miRNA-pathway network (Fig. 6A–C). Additionally, a TF-miRNA network was established on the basis of the 31 known differentially expressed miRNAs and their predicted TFs (Fig. 6D). Through the 4 regulatory networks, we demonstrated that the miRNAs not only exert their complex functions through regulating their target genes and the associated GOs and pathways but also are themselves mediated by various TFs.

3.6. Hierarchical GO category analysis, co-expression network analysis and detection of target genes involved in immune system processes

Further, we specifically looked into the hierarchical GO categories of the deregulated miRNA-associated targets with the immune system processes derived from the above biological process analyses. In the biological process categories produced by the GO analysis, 20 known differentially expressed miRNAs and 48 targets were found to participate in immune system processes (Table 4). Moreover, these targets were submitted to a hierarchical GO categories analysis, and the results showed that the 48

targets were involved in 5 key subsets of biological processes, including macrophage activation, antigen processing and presentation, response to interferon-gamma, B cell-mediated immunity and complement activation (Fig. 7A). Hence, we proposed that the 20 known differentially expressed miRNAs could indirectly mediate these biological processes and might be the crucial factors resulting in the differences between EV71 and CA16 infection. In addition, the corresponding targets of the 20 known differentially expressed miRNAs were used to build a co-expression network (Fig. 7B), which contained cytokines (e.g., IL-15 and IL-21), chemokines (e.g., CX3CL1 and CCL18), Toll-like receptors (e.g., TLR4) and NF-κB signalling-related molecules (e.g., IRAK1, IRAK2, TRAF6 and TRAF4), among others. These targets and co-expression genes might provide new information regarding the underlying distinct mechanisms caused by EV71 and CA16 infection.

Subsequently, we randomly chose 16 of the 48 targets to further measure to confirm the miRNA sequencing data. In general, the expression levels of these miRNAs and their targets presented an inverse relationship based on the regulatory mechanisms of the miRNAs. Except for EDNRB and ROBO2, the expression levels of target genes were inversely correlated with the expression patterns of the miRNAs regulating these target genes (Supplementary Fig. S6 in the online version at DOI: 10.1016/j.biocel.2016.10.011).

3.7. The regulatory role of miR-146b-5p on its targets and downstream pro-inflammation cytokines in CD1c+DCs subjected to EV71 and CA16 infection

miR-146, as an immune system regulator, influences the mammalian response to microbial and virus infection (Ma et al., 2011). As shown in Supplementary Fig. S7 in the online version at DOI: 10.1016/j.biocel.2016.10.011, miR-146b-5p was decreased in CD1c+DCs with EV71 infection, its target genes (IRAK1 and TRAF6) were up-regulated, and the corresponding downstream molecules (TNF-α, IL-1β, IL-6) were activated. However, the expression levels of these mRNAs and miR-146b-5p were opposite in CD1c+DCs following CA16 infection. Therefore, this result further illustrated
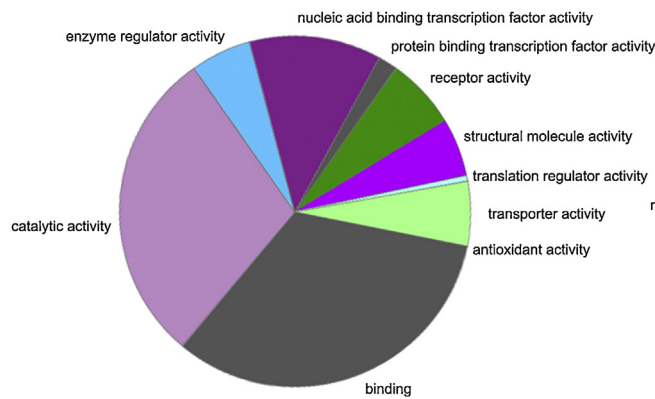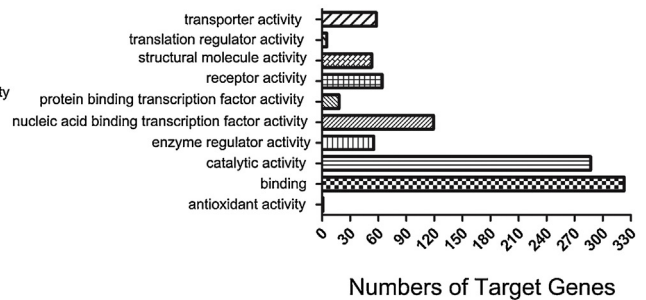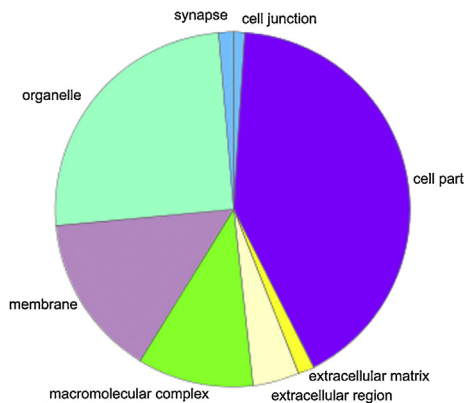
A，Biological Process
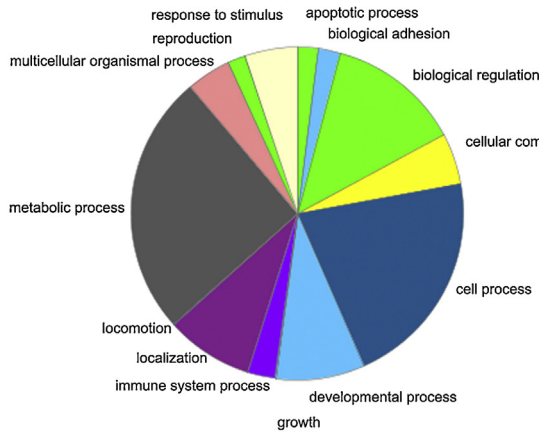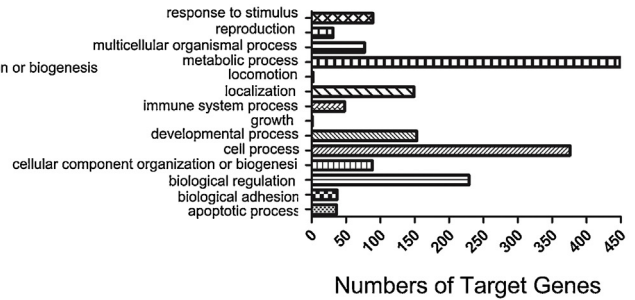
B，Molecular Function
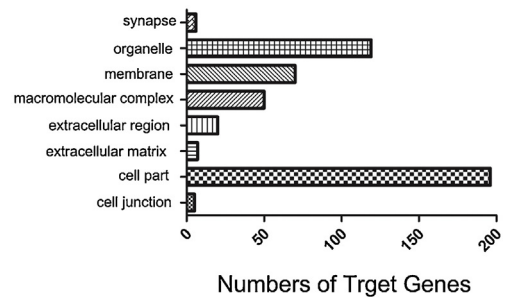

C，Cellular Component

Fig. 4. Gene Ontology enrichment terms for putative miRNA targets. Pie charts of the enriched biological processes (A), molecular functions (B) and cellular components (C) generated from the putative targets of the 32 key differentially expressed miRNAs. Bars indicate the number of GOs annotated as unique GO terms and are presented in the right panel.

that EV71 infection might trigger the immune response, while CA16 infection might impede the immune response.

4. Discussion

HFMD, which is predominantly caused by EV71 and CA16, has emerged as a serious public health threat across the Asia-Pacific region (Koh et al., 2016). Although an inactivated EV71 vaccine was found to be safe and to elicit strong protection against EV71 infection, the vaccine does not protect against CA16 infection (Liu et al., 2014a). Therefore, further investigations into the factors that cause different responses to EV17 and CA16 infections may provide new strategies for the development of more efficacious vaccines to prevent HFMD outbreaks. In this study, we found that a total of 106
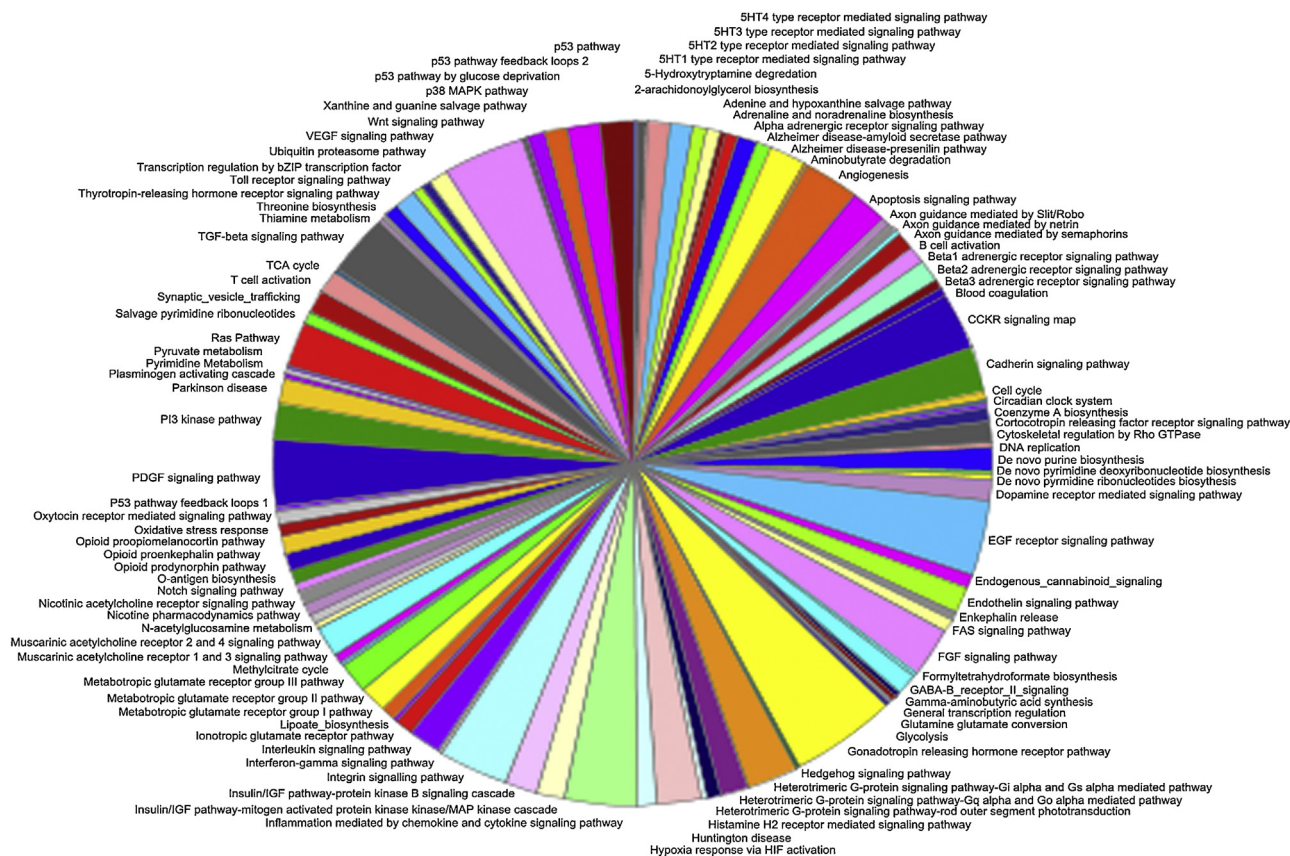
Fig. 5. KEGG pathway analysis of the predicted targets of differentially expressed miRNAs. There are 104 pathways in total, as depicted in the pie chart.

known and 13 novel miRNAs significantly changed in PBMCs following EV71 and CA16 infection, and of these, both common and unique miRNAs were identified. miRNAs are pivotal gene regulators that act on mRNAs to cause either translation inhibition or mRNA degradation, and they participate in numerous physiological and pathological processes (Ha and Kim, 2014; Sidhu et al., 2015). Hence, it is not surprising that abnormal miRNA expression may result in the pathogenesis of multiple diseases. Growing evidence has indicated that most virus infections alter the expression of cellular miRNA and that cellular miRNAs can modulate viral pathogenesis and replication by regulating the expression of viral or host genes (Roberts et al., 2011; Sullivan and Ganem, 2005). For instance, notable changes in cellular miRNAs expression levels were found in response to hepatitis C virus (HCV) infection (Li et al., 2016). Among these differentially expressed miRNAs, miR-122 was found to facilitate HCV replication by promoting the colony formation efficiency of the virus (Shan et al., 2007), whereas miR-196 substantially attenuated virus replication by directly targeting the HCV genome or indirectly binding to Bach1 (Hou et al., 2010). Many studies have also been conducted to explore the effects of miRNAs on EV71 infection. Cui et al. revealed that host miRNA expression patterns were altered in response to EV71 infection in Hep2 cells, which implied that certain miRNAs might be involved in the pathogenesis of EV71 infection (Cui et al., 2010). Another study reported a dramatic reduction in EV71 replication when DGCR8 (an essential cofactor for miRNA biogenesis) was knocked down prior to EV71 infection, which demonstrated that EV71 might utilize host miRNAs to enhance virus replication (Lui et al., 2014). Additionally, it was reported that some miRNAs show differential expression levels following EV71 and CA16 infection and that three key miRNAs (miR-545, miR-324-3p, and miR-143) can be used to distinguish EV71 infection from CA16 infection in patients with HFMD (Cui

et al., 2011). Together with these studies, our study demonstrated two important points: 1) differential miRNA expression profiles are produced at different time points following EV71 and CA16 infection; and 2) alterations of common and unique differentially expressed miRNAs following EV71 and CA16 infection can be used as diagnostic markers and may be therapeutic targets that are worth exploration. Therefore, in order to further determine the key disparities between EV71 and CA16 infection, we identified 32 differentially expressed miRNAs that displayed an inverse expression trend between infections with the two viruses. Many studies have indicated that these 32 miRNAs function in various diseases. For example, let-7e-5p was shown to increase the migration and tube formation of human endothelial progenitor cells by targeting Fas ligand (FASLG), resulting in deep vein thrombosis (DVT); therefore, let-7e-5p could be a potential therapeutic target in DVT treatment (Kong et al., 2016). miRNA-182 can exacerbate cerebral ischaemia injury by inhibiting expression of inhibitory member of the apoptosis-stimulating proteins of p53 family (iASPP); therefore, a novel miRNA-182-mediated mechanism may provide new therapeutic opportunities to enhance neuronal survival in cerebral ischaemia injury (Yi et al., 2016). miRNA-301a-3p can aggravate pancreatic ductal adenocarcinoma (PDAC) progression by suppressing the target gene SMAD4 and is therefore regarded as an independent prognostic factor for worse survival (Xia et al., 2015). miRNA-204, which has frequently been investigated in different types of cancers, acts as a tumour suppressor in colorectal cancer by repressing RAB22A, a member of the RAS oncogene family (Yin et al., 2014). However, the roles of differentially expressed miRNAs in the pathogeneses of EV71 and CA16 infection were not known and required further investigation.

To further understand the molecular pathogenesis of EV71 and CA16, we performed GO and pathway analysis of the potential tar-
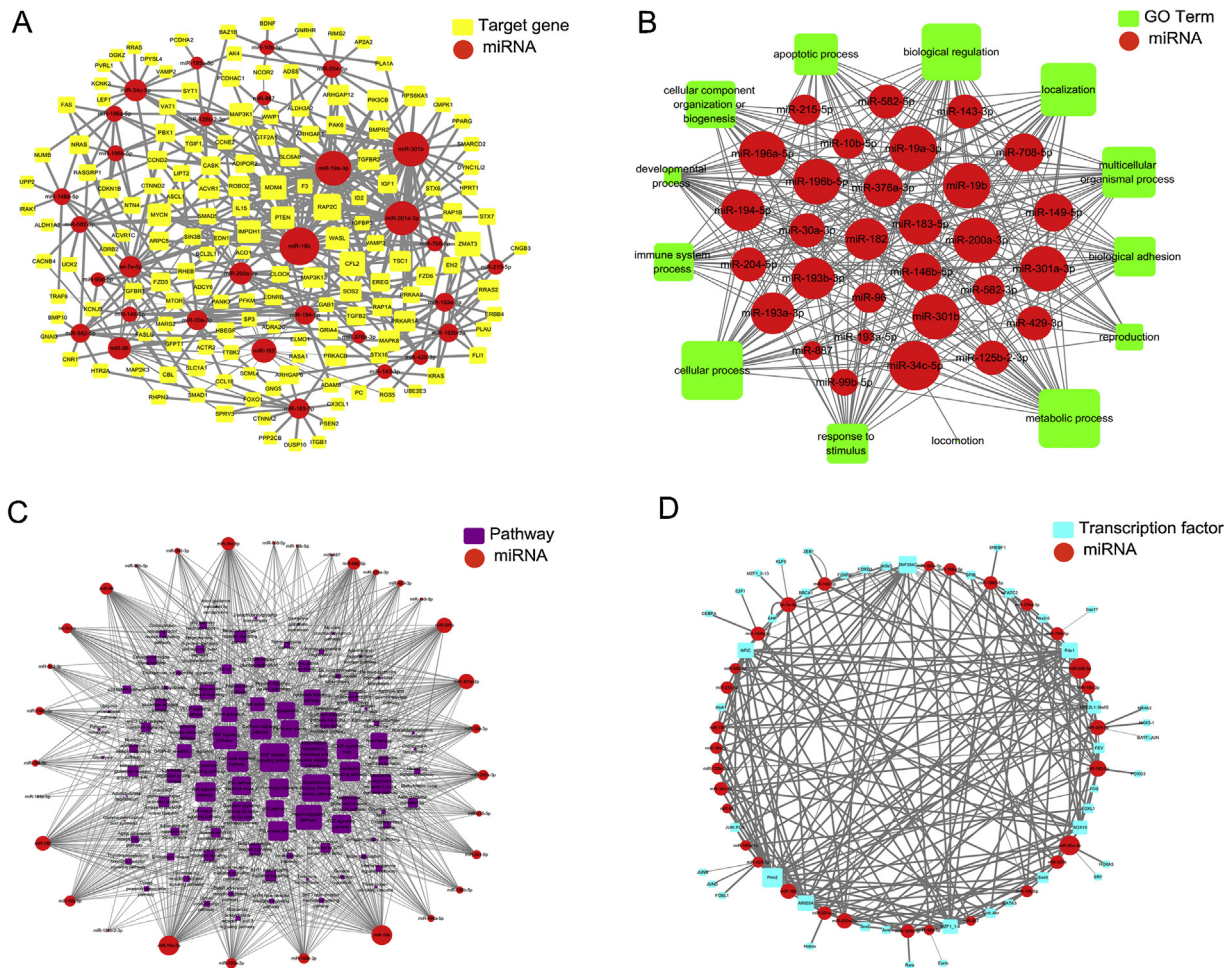
Fig. 6. Predicted networks between the oppositely expressed miRNAs and their putative target genes, their putative target gene-associated GOs, their putative target gene-associated pathways, and their putative TFs. All miRNAs are depicted as a red colored node among 4 networks. The larger the area of the nodes, the bigger the number of connections between a miRNA and other nodes in the network. (A) Predicted network between the oppositely expressed miRNAs and their putative target genes. Putative targets are presented yellow rounded rectangles. The width of the line represents the free energy between the miRNAs and their putative target genes. (B) Predicted network between the oppositely expressed miRNAs and their putative target gene-associated GOs. Green rectangle nodes denote miRNAs and GOs. Edges show the inhibitory effects of miRNAs on GOs. (C) Predicted network between the oppositely expressed miRNAs and their putative target gene-associated pathways. Pathways are depicted as purple colored nodes. The lines indicate the negative regulatory functions of miRNAs on pathways. (D) Light blue rounded rectangles represent TFs. The grey lines between the miRNAs and their putative TFs reflect correlations above the threshold of 0.99, with thickness proportional to the magnitude of correlation. (For interpretation of the references to colour in this figure legend, the reader is referred to the web version of this article.)

gets of 32 differentially expressed miRNAs. In this analysis, the predicted functions of the targets were classified into biological process, molecular function, and cellular component categories. The observed changes in biological processes (especially related to apoptotic processes and immune system processes) and pathways (especially associated with immune pathways, such as the apoptosis signalling pathway, the Toll-receptor signalling pathway, T cell activation, interleukin signalling, interferon-gamma signalling, inflammation mediated by chemokine and cytokine signalling, the FAS signalling pathway and B cell activation) suggested that the regulation of these miRNAs plays important roles in modulating immune responses and the viral pathogenesis of EV71 and CA16 infection. Additionally, an increasing number of studies have verified that miRNAs play a critical role in regulating the immune response, including the differentiation, proliferation, cell fate determination, and function of immune cells as well as in inflammatory mediator release and in modulating intracellular signalling pathways (Sonkoly et al., 2008; Winter, Jung, 2009). Hence, the identification of miRNAs involved in immune response processes is essential for identifying miRNA regulatory mechanisms. Consequently, the current study's establishment of

regulatory networks provides new insights into the interactions that form between miRNAs and targets, miRNAs and GOs, miRNAs and signalling pathways, and miRNAs and TFs, all of which contribute to the viral pathogenesis.

Virus-host interactions largely determine the pathological outcome of infection (Sullivan and Ganem, 2005). The innate immune system, as an early defence, responds immediately to the presence of pathogens and can effectively activate antiviral programs that serve to limit virus replication. This activation also elicits the adaptive immune response, which initiates clearance of infectious organisms (Xiao and Rajewsky, 2009). Therefore, a focus was placed on the immune system processes originating from the GO analysis for deeper hierarchical GO category analysis in this work. Our results demonstrated that miRNAs implicated in immune system processes were consistently down-regulated following EV71 infection and up-regulated following CA16 infection. Moreover, based on the theory that miRNAs are natural antisense interactors that regulate their target genes, miRNAs can also exert a negative regulatory effect on the corresponding GO categories of their target genes. Thus, the functions of these hierarchical GO categories, including macrophage activation, antigen processing and presen-
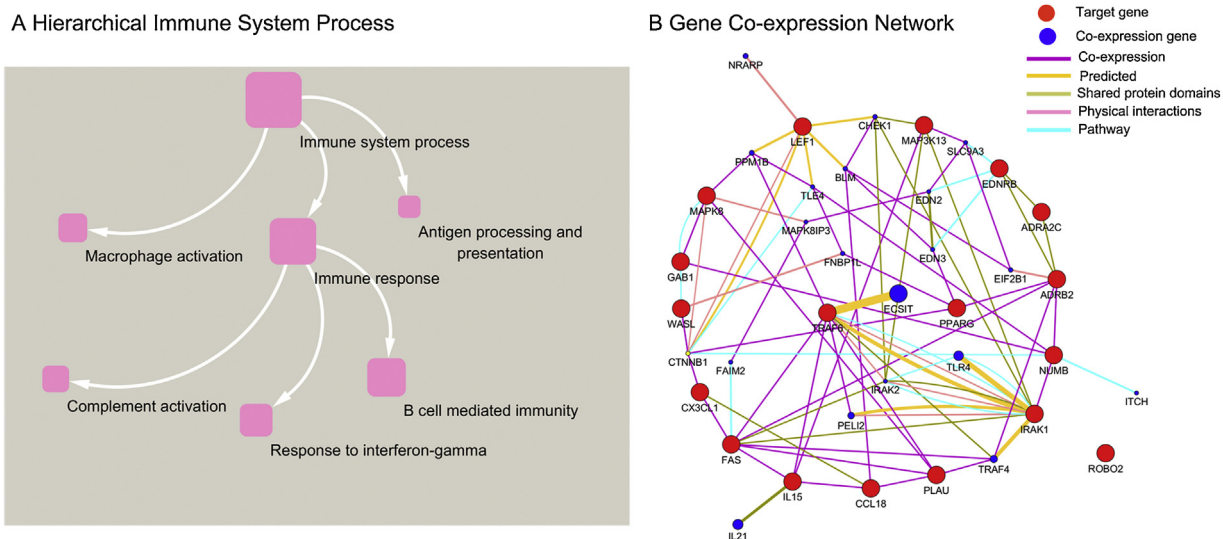
Fig. 7. Hierarchical tree graphs of GO terms and co-expression network for genes involved in immune system processes. (A) In total, 48 genes were used to generate the GO tree. Edges represent "parent-child" relationships of GO terms. The sizes of the pink rounded rectangles are proportional to the number of GO terms annotated to each node. (B) Co-expression network were constructed by immune-related targets. Red nodes are target genes and blue nodes are co-expression genes. Genes with bigger size are more centralized in the network and have a stronger capacity of modulating adjacent genes. Different color lines mean the different interactions between these genes. (For interpretation of the references to colour in this figure legend, the reader is referred to the web version of this article.)

tation, response to interferon-gamma, B cell-mediated immunity and complement activation, might be activated during EV71 infection and inhibited during CA16 infection. It was also confirmed by qRT-PCR analysis that most target genes involved in immune system processes had increased expression during EV71 infection and decreased expression during CA16 infection. This result indirectly suggests that there is a negative correlation between these differentially expressed miRNAs related to immune system processes and their target genes during EV71 and CA16 infection. To the best of our knowledge, the above-mentioned GO terms are the central elements of the innate immune response and adaptive immune response, which are the universal mechanisms of host defence against infection. As a result, the identification of these processes by hierarchical GO category analysis implied that remarkable differences are present in the innate and adaptive immune responses that are induced by EV71 and CA16 infection. Additionally, the effects of the above miRNAs (such as let-7e-5p and miRNA-146b-5p) on immune responses have been previously reported. Dong et al. revealed that down-regulating the expression of let-7e-5p triggered the activation of IFN-α signalling in B cells, playing a role in the pathogenesis of systemic lupus erythematosus (SLE) through the production of pathogenic auto-antibodies (Dong et al., 2015). In the current study, we found that let-7e-5p expression was obviously reduced during EV71 infection and increased during CA16 infection; therefore, we hypothesized that EV71 infection, but not CA16 infection, stimulates B cells to produce antibodies. An increasing number of studies have verified that miRNA-146b-5p is involved in various cancers and inflammatory diseases through its targeting of the TRAF6 and IRAK1 genes, which are the key adaptor molecules of the NF-κB signalling pathway (Al-Ansari and Aboussekhra, 2015; Liu et al., 2015). Much accumulated evidence has supported that miRNAs play an important role in the regulation of the NF-κB signalling pathway during viral infections (Gao et al., 2014) and that the NF-κB signalling pathway is critical to innate and adaptive immunity, inflammation, and tumour development Ma et al., 2011). Moreover, our co-expression network result showed that some targets (TRAF6, IRAK1, MAP3K13, MAPK8, etc.) and co-expression molecules (TLR4, IRAK2, TRAF4, etc.) involved in the NF-κB signalling pathway may contribute to the differences observed in EV71 and CA16 infection. Addition-

ally, we found that miR-146b-5p was down-regulated in CD1c⁺DCs infected with EV71, resulting in a decrease of IRAK1 and TRAF6 as well as a corresponding inhibition of downstream genes, including TNF-α, IL-1β, IL-6, while the opposite expression patterns of miR-146b-5p, IRAK1, TRAF6, TNF-α, IL-1β and IL-6 were observed in CD1c⁺DCs infected with CA16. Hence, the decreased expression of miRNA-146b-5p during EV71 infection initiated the innate immune response, whereas the increased expression of miRNA-146b-5p during CA16 infection inhibited the innate immune response. Taken together, these findings provide a possible explanation for the distinct clinical symptoms that result from EV71 and CA16 infection.

In conclusion, this study demonstrated for the first time that EV71 and CA16 infections result in specific miRNA expression patterns in PBMCs. More studies are needed to dissect the relevant roles of miRNAs in viral pathogenesis. Furthermore, we constructed regulatory networks of differentially expressed miRNAs screened from trend analysis, providing a global perspective for exploring miRNA-mediated mechanisms. Finally, our results demonstrated that the 20 known differentially expressed miRNAs involved in immune system processes that were identified in this study are the key miRNAs that underlie the different immune responses induced by EV71 and CA16 infection.

Conflict of interest

The authors do not have any commercial or other associations that might pose a conflict of interest.

Acknowledgments

References

Al-Ansari, M.M., Aboussekhra, A., 2015. miR-146b-5p mediates p16-dependent repression of IL-6 and suppresses paracrine procarcinogenic effects of breast stromal fibroblasts. Oncotarget 6, 30006–30016.

Aswathyraj, S., Arunkumar, G., Alidjinou, E.K., Hober, D., 2016. Hand, foot and mouth disease (HFMD): emerging epidemiology and the need for a vaccine strategy. Med. Microbiol. Immunol. (Berl) 205, 397–407.

Carissimi, C., Fulci, V., Macino, G., 2009. MicroRNAs: novel regulators of immunity. Autoimmun. Rev. 8, 520–524.

Cui, L., Guo, X., Qi, Y., Qi, X., Ge, Y., Shi, Z., et al., 2010. Identification of microRNAs involved in the host response to enterovirus 71 infection by a deep sequencing approach. J. Biomed. Biotechnol. 2010, 425939.

Cui, L., Qi, Y., Li, H., Ge, Y., Zhao, K., Qi, X., et al., 2011. Serum microRNA expression profile distinguishes enterovirus 71 and coxsackievirus 16 infections in patients with hand-foot-and-mouth disease. PLoS One 6, e27071.

Delves, P., Martin, S., Burton, D., 2006. I.R. Roitt's Essential Immunology. Blackwell Science, Oxford.

Dong, G., Fan, H., Yang, Y., Zhao, G., You, M., Wang, T., et al., 2015. 17beta-Estradiol enhances the activation of IFN-alpha signaling in B cells by down-regulating the expression of let-7e-5p, miR-98-5p and miR-145a-5p that target IKKepsilon. Biochim. Biophys. Acta 1852, 1585–1598.

Gao, Z., Dou, Y., Chen, Y., Zheng, Y., 2014. MicroRNA roles in the NF- kappaB signaling pathway during viral infections. BioMed Res. Int. 2014, 436097.

Ha, M., Kim, V.N., 2014. Regulation of microRNA biogenesis. Nat. Rev. Mol. Cell Biol. 15, 509–524.

Ho, B.C., Yang, P.C., Yu, S.L., 2016. MicroRNA and pathogenesis of enterovirus infection. Viruses 8.

Hou, W., Tian, Q., Zheng, J., Bonkovsky, H.L., 2010. MicroRNA-196 represses Bach1 protein and hepatitis C virus gene expression in human hepatoma cells expressing hepatitis C viral proteins. Hepatology 51, 1494–1504.

Koh, W.M., Bogich, T., Siegel, K., Jin, J., Chong, E.Y., Tan, C.Y., et al., 2016. The epidemiology of hand, foot and mouth disease in asia: a systematic review and analysis. Pediatr. Infect. Dis. J. 35, e285–300.

Kong, L., Du, X., Hu, N., Li, W., Wang, W., Wei, S., et al., 2016. Downregulation of let-7e-5p contributes to endothelial progenitor cell dysfunction in deep vein thrombosis via targeting FASLG. Thromb. Res. 138, 30–36.

Lee, T.C., Guo, H.R., Su, H.J., Yang, Y.C., Chang, H.L., Chen, K.T., 2009. Diseases caused by enterovirus 71 infection. Pediatr. Infect. Dis. J. 28, 904–910.

Lee, H.M., Nguyen, D.T., Lu, L.F., 2014. Progress and challenge of microRNA research in immunity. Front. Genet. 5, 178.

Lewis, B.P., Shih, I.H., Jones-Rhoades, M.W., Bartel, D.P., Burge, C.B., 2003. Prediction of mammalian microRNA targets. Cell 115, 787–798.

Li, J.X., Mao, Q.Y., Liang, Z.L., Ji, H., Zhu, F.C., 2014a. Development of enterovirus 71 vaccines: from the lab bench to Phase III clinical trials. Expert Rev. Vacc. 13, 609–618.

Li, R., Liu, L., Mo, Z., Wang, X., Xia, J., Liang, Z., et al., 2014b. An inactivated enterovirus 71 vaccine in healthy children. N. Engl. J. Med. 370, 829–837.

Li, H., Jiang, J.D., Peng, Z.G., 2016. MicroRNA-mediated interactions between host and hepatitis C virus. World J. Gastroenterol. 22, 1487–1496.

Liu, C.C., Chow, Y.H., Chong, P., Klein, M., 2014a. Prospect and challenges for the development of multivalent vaccines against hand, foot and mouth diseases. Vaccine 32, 6177–6182.

Liu, W., Wu, S., Xiong, Y., Li, T., Wen, Z., Yan, M., et al., 2014b. Co-circulation and genomic recombination of coxsackievirus A16 and enterovirus 71 during a large outbreak of hand, foot, and mouth disease in Central China. PLoS One 9, e96051.

Liu, J., Xu, J., Li, H., Sun, C., Yu, L., Li, Y., et al., 2015. miR-146b-5p functions as a tumor suppressor by targeting TRAF6 and predicts the prognosis of human gliomas. Oncotarget 6, 29129–29142.

Louten, J., Beach, M., Palermino, K., Weeks, M., Holenstein, G., 2015. MicroRNAs expressed during viral infection: biomarker potential and therapeutic considerations. Biomark. Insights 10, 25–52.

Lui, Y.L., Tan, T.L., Woo, W.H., Timms, P., Hafner, L.M., Tan, K.H., et al., 2014. Enterovirus71 (EV71) utilise host microRNAs to mediate host immune system enhancing survival during infection. PLoS One 9, e102997.

Ma, X., Becker Buscaglia, L.E., Barker, J.R., Li, Y., 2011. MicroRNAs in NF-kappaB signaling. J. Mol. Cell Biol. 3, 159–166.

Malone, J.H., Oliver, B., 2011. Microarrays, deep sequencing and the true measure of the transcriptome. BMC Biol. 9, 34.

Mao, Q., Wang, Y., Yao, X., Bian, L., Wu, X., Xu, M., et al., 2014. Coxsackievirus A16: epidemiology, diagnosis, and vaccine. Hum. Vacc. Immunother. 10, 360–367.

McMinn, P.C., 2002. An overview of the evolution of enterovirus 71 and its clinical and public health significance. FEMS Microbiol. Rev. 26, 91–107.

Muehlenbachs, A., Bhatnagar, J., Zaki, S.R., 2015. Tissue tropism, pathology and pathogenesis of enterovirus infection. J. Pathol. 235, 217–228.

Powdrill, M.H., Desrochers, G.F., Singaravelu, R., Pezacki, J.P., 2016. The role of microRNAs in metabolic interactions between viruses and their hosts. Curr. Opin. Virol. 19, 71–76.

Roberts, A.P., Lewis, A.P., Jopling, C.L., 2011. The role of microRNAs in viral infection. Prog. Mol. Biol. Transl. Sci. 102, 101–139.

Shan, Y., Zheng, J., Lambrecht, R.W., Bonkovsky, H.L., 2007. Reciprocal effects of micro-RNA-122 on expression of heme oxygenase-1 and hepatitis C virus genes in human hepatocytes. Gastroenterology 133, 1166–1174.

Sharma, N., Singh, S.K., 2016. Implications of non-coding RNAs in viral infections. Rev. Med. Virol. 26, 356–368.

Sidhu, K., Kapoor, N.R., Pandey, V., Kumar, V., 2015. The macro world of microRNAs in hepatocellular carcinoma. Front. Oncol. 5, 68.

Solomon, T., Lewthwaite, P., Perera, D., Cardosa, M.J., McMinn, P., Ooi, M.H., 2010. Virology, epidemiology, pathogenesis, and control of enterovirus 71. Lancet Infect. Dis. 10, 778–790.

Song, J., Hu, Y., Hu, Y., Wang, J., Zhang, X., Wang, L., et al., 2016. Global gene expression analysis of peripheral blood mononuclear cells in rhesus monkey infants with CA16 infection-induced HFMD. Virus Res. 214, 1–10.

Sonkoly, E., Stahle, M., Pivarcsi, A., 2008. MicroRNAs and immunity: novel players in the regulation of normal immune function and inflammation. Semin. Cancer Biol. 18, 131–140.

Sullivan, C.S., Ganem, D., 2005. MicroRNAs and viral infection. Mol. Cell 20, 3–7.

Winter, J., Jung, S., Keller, S., Gregory, R.I., Diederichs, S., 2009. Many roads to maturity: microRNA biogenesis pathways and their regulation. Nat. Cell Biol. 11, 228–234.

Wong, N., Wang, X., 2015. miRDB: an online resource for microRNA target prediction and functional annotations. Nucleic Acids Res. 43, D146–52.

Xia, X., Zhang, K., Cen, G., Jiang, T., Cao, J., Huang, K., et al., 2015. MicroRNA-301a-3p promotes pancreatic cancer progression via negative regulation of SMAD4. Oncotarget 6, 21046–21063.

Xiao, C., Rajewsky, K., 2009. MicroRNA control in the immune system: basic principles. Cell 136, 26–36.

Yi, H., Huang, Y., Yang, F., Liu, W., He, S., Hu, X., 2016. MicroRNA-182 aggravates cerebral ischemia injury by targeting inhibitory member of the ASPP family (iASPP). Arch. Biochem. Biophys. 9861, 30141–30142.

Yin, Y., Zhang, B., Wang, W., Fei, B., Quan, C., Zhang, J., et al., 2014. miR-204-5p inhibits proliferation and invasion and enhances chemotherapeutic sensitivity of colorectal cancer cells by downregulating RAB22A. Clin. Cancer Res. 20, 6187–6199.

Zhang, Y., Yang, E., Pu, J., Liu, L., Che, Y., Wang, J., et al., 2014. The gene expression profile of peripheral blood mononuclear cells from EV71-infected rhesus infants and the significance in viral pathogenesis. PLoS One 9, e83766.